APL Photonics

RESEARCH ARTICLE | JULY 28 2025

The influence of subwavelength geometry on extracting the electrical properties of semiconductors by terahertz spectroscopy

Ford M. Wagner ; Tuomas Haggren ; Jasmin-Clara Bürger ; Terng Junn Keat ; Kun Peng ; Chawit Uswachoke ; Djamshid A. Damry; Hans Kraus; Hannah J. Joyce ; Hark Hoe Tan ; Chennupati Jagadish ; Thomas Siday ; Michael B. Johnston

APL Photonics 10, 076123 (2025)
https://doi.org/10.1063/5.0273919

The influence of subwavelength geometry on extracting the electrical properties of semiconductors by terahertz spectroscopy

Cite as: APL Photon. 10, 076123 (2025); doi: 10.1063/5.0273919
Submitted: 2 April 2025 • Accepted: 28 June 2025 •
Published Online: 28 July 2025

Ford M. Wagner,[1] Tuomas Haggren,[2] Jasmin-Clara Bürger,[1] Terng Junn Keat,[1] Kun Peng,[1] Chawit Uswachoke,[3] Djamshid A. Damry,[1] Hans Kraus,[1] Hannah J. Joyce,[3] Hark Hoe Tan,[2] Chennupati Jagadish,[2] Thomas Siday,[1,4,a)] and Michael B. Johnston[1,b)]

AFFILIATIONS

[1] Department of Physics, Clarendon Laboratory, University of Oxford, Parks Road, Oxford OX1 3PU, United Kingdom
[2] ARC Centre of Excellence for Transformative Meta-Optical Systems, Department of Electronic Materials Engineering, Research School of Physics, The Australian National University, Canberra, ACT 2601, Australia
[3] Electrical Engineering Division, Department of Engineering, University of Cambridge, Cambridge CB3 0FA, United Kingdom
[4] School of Physics and Astronomy, University of Birmingham, Edgbaston, Birmingham B15 2TT, United Kingdom

[a)] **E-mail:** t.siday@bham.ac.uk
[b)] **Author to whom correspondence should be addressed:** michael.johnston@physics.ox.ac.uk

ABSTRACT

Terahertz (THz) spectroscopy is a non-contact technique well-suited for probing the ultrafast electrical conductivity of semiconductor nanostructures, where conventional methods are often impractical. However, geometric resonances in these nanostructures can distort the measured THz response, complicating the extraction of the intrinsic material properties. Here, we use THz spectroscopy to study GaAs nanowires of varying lengths and observe that the resonant frequency increases as the nanowire length decreases. Further measurements on a model system of well-defined GaAs microsquares (ranging in size from 500 × 500 to 7 × 7 μm^2) confirmed the relationship between structure size and resonant frequency. We verify that a plasmon-based model successfully separates the geometric response from the intrinsic charge-carrier response. Thus, the model allows for the accurate evaluation of critical material properties in nanostructured semiconductors, such as electron mobility. Fluence-dependent measurements and finite-difference time-domain simulations confirm the plasmonic nature of the resonances.

I. INTRODUCTION

The miniaturization of semiconductors has driven improvements in technology and enabled access to new phenomena at the micro- and nanoscales. For example, semiconductor nanowires pair excellent charge transport properties with nanoscale dimensions, making them promising candidates as the building blocks of future optoelectronics,[1–5] while semiconductor metasurfaces utilize nanostructures for the tunable manipulation of light.[6–9] Other emerging material systems—such as metal-halide perovskite semiconductors—form nanoscale grains, with studies showing that larger grains lead to improved charge transport owing to reduced charge-carrier scattering at grain boundaries.[10–12]

Optimization of structured semiconductor devices requires a sound understanding of their intrinsic charge-carrier dynamics. However, the microscale/nanoscale dimensions of such structures make conventional characterization methods difficult and impractical to conduct. For example, Hall effect measurements require electrical contacts to be fabricated on the sample.[13] The contact fabrication process is extremely difficult and time-consuming at the nanoscale and can contaminate the sample, altering its properties. Hence, alternative characterization tools are required to study accurately the properties of structured semiconductors.

Terahertz (THz) spectroscopy is an ideal tool to study micro- and nanostructured semiconductors with ultrafast time resolution.[14,15] It is a contact-free technique that allows for high-throughput measurements of the pristine semiconductor. Furthermore, THz radiation (0.1–30 THz) is sensitive to processes with sub-picosecond lifetimes, which makes it an excellent probe of charge-carrier transport in semiconductors. An optical pump pulse can be used to photoexcite the sample, such that the THz pulse probes the material's photoconductivity.[16]

THz spectroscopy has been used to study a range of different structured semiconductors, including nanoparticles,[17,18] nanowires,[2–4,19] and nanobars.[20] The conductivity spectrum for these materials includes a resonance—a large deviation from the free-electron response (Drude) of the corresponding bulk semiconductors.[21–24] This resonance is the result of the sample geometry and is not part of the intrinsic carrier response.[25] Such structural resonances must be carefully treated in the analysis to ensure that the spectra are correctly interpreted and any extracted properties are representative of the material.

Here, we investigate whether the influence of micro- and nanoscale structure can be separated from the intrinsic THz carrier dynamics of materials. We begin by studying GaAs nanowires of different lengths to establish the microscopic (physical) mechanism behind the resonances and to gain insight about the influence of size. We then move to a well-defined system of microsquare arrays fabricated from GaAs thin film, which range in size from 500 × 500 to 7 × 7 μm^2. An increase in resonant frequency was observed as the size of the microsquares decreased, which mirrored the result observed in the length-dependent nanowires. We verify the surface plasmon model as a method to accurately separate the intrinsic response of the GaAs from the response of the geometry. In particular, we focus on extracting the charge-carrier mobility from the GaAs, as it is an important material property for device applications. We conducted carrier-density dependent measurements on the microsquares and employed finite-difference time-domain (FDTD) simulations to confirm the plasmonic nature of the resonances in the conductivity spectra.

II. RESULTS AND DISCUSSION

A. Length dependence of nanowires on THz photoconductivity spectra

Semiconductor nanowires are prototypical nanostructures with a one-dimensional geometry that can host structural resonances in the THz range.[26,27] Hence, we first explore the relationship between geometric resonances and nanostructure size through THz photoconductivity measurements of GaAs nanowires of different lengths. Three sets of nanowires were grown epitaxially on GaAs substrates to different lengths (details in the supplementary material) before being mechanically transferred onto quartz substrates for measurement. This transfer method ensured the nanowires were reasonably well aligned, minimizing the effects of nanowire polarization anisotropy on the photoconductivity spectra.[28,29] However, this transfer process also broke the nanowires, resulting in a distribution of nanowire lengths on each sample. We refer to each sample by the mode of the nanowire length after substrate transfer: 0.5, 2, and 3 μm. Figure 1(a) shows a schematic diagram of the THz

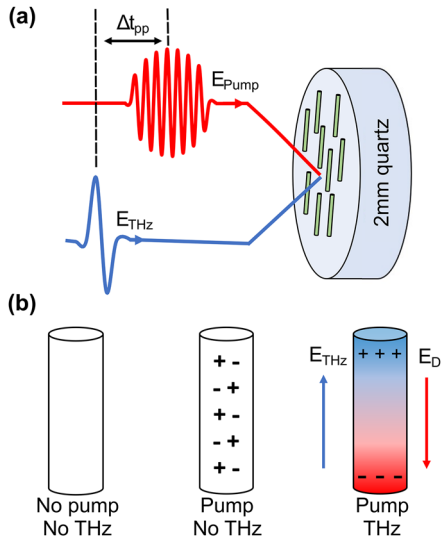

FIG. 1. (a) Schematic diagram of the measurements on nanowire arrays. The 800-nm, 35-fs laser pump pulse excites the nanowires some time, Δt_{pp}, before the THz pulse arrives to probe the photoexcited properties of the nanowires. (b) Schematic diagrams of the free charge-carrier density in a nanowire before and after the pump and THz pulses have interacted with the nanowire. The final diagram illustrates the accumulation of charges because of the THz electric field (E_{THz}) acting on the nanowire geometry and the associated depolarization field (E_D).

photoconductivity measurements with respect to the nanowire sample geometry.

The nanowire photoconductivity was calculated using an effective medium approach[19] (described in the supplementary material) with fill factors determined by analysis of optical microscope images. The photoconductivity spectra are presented in Fig. 2(a). There is a clear resonance in all the spectra that shifts toward higher frequencies as the mode of the nanowire length decreases. This relationship between nanowire length and resonant frequency is consistent with simulations,[30] effective medium models,[1,31] and experiments in the mid-IR on silicon nanowires.[32]

It is important to note that there is a large range of nanowire lengths in each sample, as shown in the SEM images of the nanowires in Fig. 2(b). Thus, it was necessary to obtain a clear picture of the nanowire length distribution before making any statements linking nanowire length to resonant frequency. We measured the nanowire length distributions from SEM images using the Fiji (ImageJ) software.[33] The length histograms are presented in Fig. 2(c) (enlarged histograms are provided in the supplementary material), with the summarized length statistics printed in Table I. Many of the SEM images showed nanowires overlapping each other, which made it impossible to determine their start and finish points. Hence, we only counted nanowires in our statistics that we could accurately measure the length of. The longer nanowires were more likely to overlap and were thus more likely to be excluded from the length distribution. As a result, our statistics are weighted toward the shorter nanowires, which likely shrinks the length difference between samples. Furthermore, the nanowires that overlap may behave similarly to a single long nanowire, as in Ref. 30, further shifting the resonant frequency.

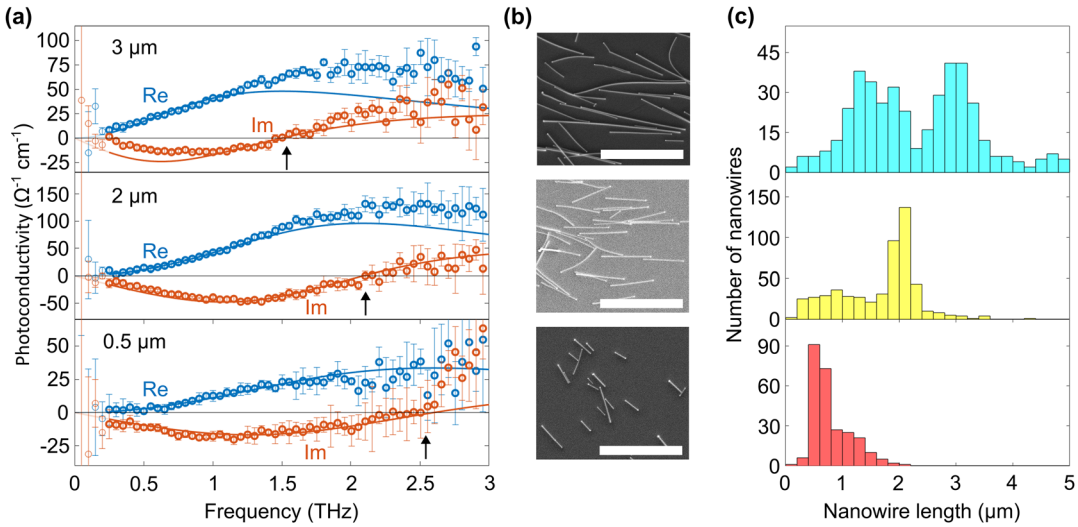

FIG. 2. (a) THz photoconductivity spectra of the three different nanowire samples, labeled by their mode length after substrate transfer. The solid lines show the fits using the surface plasmon model [Eq. (1)], and the arrows indicate the resonant frequencies. Data were measured 0.5 ps after photoexcitation with a pump beam fluence of 395 μJ cm^{-2}. (b) SEM images of the nanowires after transfer and (c) histograms of the nanowire length distribution for each sample. Panels (b) and (c) are aligned horizontally with their corresponding photoconductivity spectrum. The scale bars in (b) are all 4 μm.

TABLE I. Statistics on the nanowire length distribution for the three nanowire samples presented in Fig. 2(b). All data were manually collected from SEM images using the Fiji software.[33]

Resonant frequency (THz)	Mode length (μm)	Median length (μm)	Mean length (μm)	Std. dev. length (μm)	Number of nanowires measured
1.50 ± 0.08	3	2.38	2.41	1.20	433
2.09 ± 0.08	2	1.91	1.66	0.69	535
2.6 ± 0.2	0.5	0.65	0.79	0.35	262

Despite these limitations, we confirm that the resonant frequency in the THz photoconductivity spectra increased as the nanowire length decreased for any chosen length statistic from Table I. Hence, our results strongly suggest a link between the nanowire length and resonant frequency.

The origin of the geometric resonance is described by Nienhuys and Sundström,[25] who developed the surface plasmon model to describe how small-scale structure can change the conductivity spectrum of a material. In this model, the standard Drude approach[1] is modified by introducing an electrostatic restoring force that acts on the charge carriers. This force arises when the incident THz pulse drives positive and negative charges in opposite directions. When the sample geometry has dimensions comparable to the THz wavelength, the charges accumulate at opposite ends, forming a transient electric dipole. The resulting internal electric field opposes the external THz electric field and is often referred to as a depolarization field.[34] This field drives harmonic oscillations of the charge carriers and leads to size-dependent resonance features in the THz spectrum. Figure 1(b) presents a schematic diagram of the formation of the depolarization field in the nanowires as the THz photoconductivity measurement proceeds. Adding the electrostatic restoring force to the Drude equation of motion results in the following equation for conductivity:

$$\sigma(\omega) = \frac{Ne^2}{m^*} \frac{i\omega}{\omega^2 - \omega_0^2 + i\omega\frac{e}{m^*\mu}}, \tag{1}$$

where N is the charge-carrier density, e is the charge of an electron, m^* is the effective mass of the charge carriers, ω is the angular frequency, ω_0 is the frequency of the resonance, and μ is the charge carrier mobility. The electrons in GaAs have an extremely small effective mass (0.063 m_e) compared to the holes (0.5 m_e), and so we assume that only electrons contribute to the conductivity in this study.[35] The Drude model is recovered when the resonant frequency is set to zero in Eq. (1). The resonant frequency is related to the charge-carrier density by

$$\omega_0 = \sqrt{\frac{gNe^2}{m^*\epsilon_0}}, \tag{2}$$

where g is a factor dependent on the sample geometry and dielectric properties, and ϵ_0 is the permittivity of free space.

We fit the surface plasmon model to the spectra in Fig. 2(a) (solid lines) and found that it agrees well with the experimental data. The fitting was completed by a non-linear least squares algorithm with three free parameters: N, ω_0, and μ. Table II shows the fit

TABLE II. Nanowire material characteristics extracted from fits of the surface plasmon model to the spectra shown in Fig. 2(a). Errors were determined by propagating the error in the nanowire fill factor.

Nanowire mode length (μm)	Fill factor	N ($\times 10^{17}$ cm^{-3})	$\omega_0/2\pi$ (THz)	μ (cm^2 V^{-1} s^{-1})
3	0.19 ± 0.07	2 ± 1	1.50 ± 0.08	1500 ± 100
2	0.14 ± 0.04	4 ± 2	2.09 ± 0.08	1500 ± 100
0.5	0.12 ± 0.03	1.9 ± 0.5	2.6 ± 0.2	1100 ± 300

parameters along with the fill factor for each sample. The charge-carrier densities strongly depend on the fill factor, which is difficult to accurately estimate in these inhomogeneous nanowire arrays; hence, the differences in N are likely due to differences between the calculated fill factor and the true fill factor of the nanowires at the measured position. The extracted mobilities are reasonably similar across all nanowire samples, which was expected as the nanowires were all fabricated by the same process, with only the growth time changing. This result demonstrates the effectiveness of Eq. (1) for modeling charge transport in nanowires and extracting their material properties.

The observed relationship between nanowire length and resonant frequency has important implications for the interpretation of THz measurements on nanowire ensembles. Notably, the width of the resonance is directly related to the nanowire charge-carrier mobility: the broader the resonance, the lower the mobility.[1] Hence, an ensemble of nanowires with varying lengths, often because of nanowires breaking during substrate transfer, will exhibit a series of resonances at slightly different frequencies corresponding to the different nanowire lengths. These different resonances will combine to form a single broad resonance in the photoconductivity spectrum, thus artificially reducing the extracted mobility of the nanowires. Therefore, the mobility of nanowire ensembles as measured by THz spectroscopy should be treated as a lower bound for the true nanowire mobility.

The artificial resonance broadening effect and the difficulty in determining fill factor and average nanowire length after substrate transfer are complications that arise from working with inhomogeneous nanowire ensembles. Our results can suggest a relationship between nanowire length and geometric resonances, but the sample inhomogeneities make it difficult to conclude anything meaningful. In order to fully understand the relationship between these resonances and structure size, it is necessary to turn our attention to a well-defined system that does not suffer from the effects of inhomogeneity.

B. A well-defined system: GaAs microsquares

To confirm the link between size and resonance in structured semiconductors, we studied a well-defined system of GaAs microsquare arrays. The microsquares were fabricated on 600-nm-thick films of GaAs by electron beam lithography (see the supplementary material for details). Each array had an active area of 5×5 mm, and the microsquares had dimensions of 500×500, 50×50, and 7×7 μm^2. To ensure electrical isolation, the microsquares were separated from one another by a 300-nm gap. After patterning, the arrays were transferred onto 2-mm-thick sapphire substrates, as sapphire offers excellent thermal conductivity and is transparent over the THz range.[22] There was a thin layer of PMMA (1.2 μm) and SU8 (800 nm) between the sapphire and

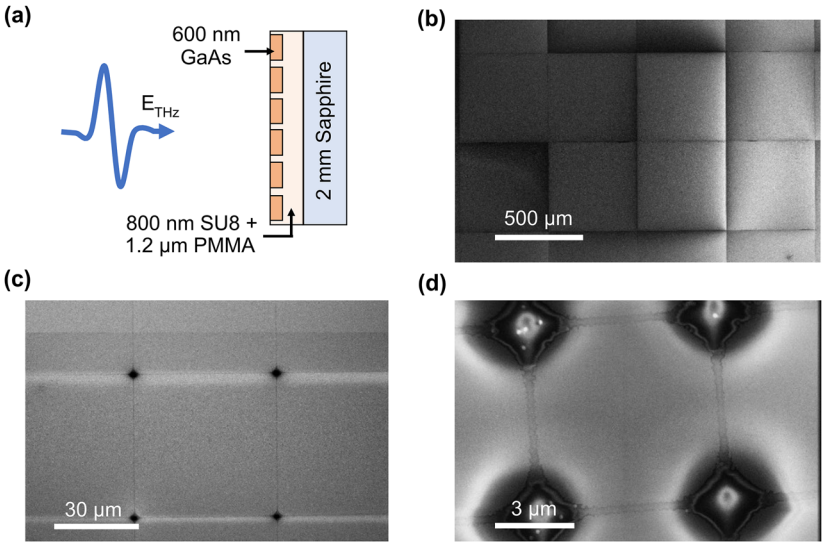

FIG. 3. (a) Schematic diagram of the GaAs microsquare sample geometry with respect to the incident THz pulse. [(b)–(d)] SEM images of the 500×500, 50×50, and 7×7 μm^2 GaAs microsquare samples, respectively.

GaAs for adhesion and lithographic purposes. A sapphire substrate with the same polymers was used as a reference to confirm that these layers did not impact any results. Figures 3(b)–3(d) show scanning electron microscope images of the microsquare arrays, and Fig. 3(a) shows a schematic diagram of the sample geometry relative to the THz pulses during measurement. A reference thin film of GaAs was created by an identical process to the microsquare arrays, except without any lithographic processing into squares. All samples share the same material properties as the reference film because they were all fabricated from identically prepared films. Hence, the microsquares are an ideal platform for this study, as we can attribute all observed differences in their photoconductivity spectra to their structural differences.

The THz photoconductivity spectra of the GaAs microsquares and reference film are shown in Fig. 4. Both the real and imaginary components of the photoconductivity for the GaAs film are always positive, and there is a peak at low frequencies. These qualities are typical of Drude conductivity, which has been shown to be an excellent description of bulk GaAs charge transport.[36] The spectrum of the 500 × 500 μm^2 microsquares is very similar to the spectrum of the GaAs film, which indicates that the geometric resonances are not clearly observed in THz measurements of structures at this scale. In contrast, the photoconductivity spectra for the 50 × 50 and 7 × 7 μm^2 microsquares show clear resonances at non-zero frequencies. The resonance is at a significantly higher frequency in the 7 × 7 μm^2 microsquares, indicating an inverse relationship between structure size and resonant frequency. This result supports our observations in the nanowires and strongly suggests a general trend in how THz conductivity spectra change with structure size.

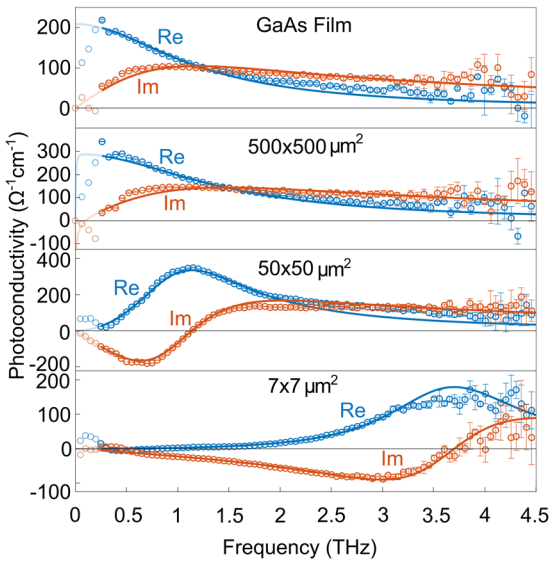

FIG. 4. THz photoconductivity spectrum of (top to bottom) a 600-nm-thick film of GaAs, a 5 × 5 mm^2 array of 500 × 500 μm^2 GaAs microsquares, 50 × 50 μm^2 GaAs microsquares, and 7 × 7 μm^2 GaAs microsquares. The circles represent the measured data, and the solid lines are the fits using the surface plasmon model [Eq. (1)]. Data below 0.25 THz (transparent data points) were excluded from the fit because they suffered from aperture-related artifacts. Data were measured 8 ps after photoexcitation by a 35-fs laser pulse with a center wavelength of 800 nm (E_{photon} = 1.55 eV) and a fluence of 23.6 $\mu J\ cm^{-2}$. All measurements were performed at room temperature in a vacuum chamber at 0.1 mbar.

We fit the surface plasmon model to the spectra shown in Fig. 4 (solid lines) and found there was excellent agreement with the experimental data, despite the very different features across the spectra. Note that the GaAs film was fitted with the Drude model [Eq. (1) with $\omega_0 = 0$] as no structure was present to allow for the formation of a depolarization field. Table III shows the extracted parameters from the surface plasmon model. Interestingly, the surface plasmon model fit suggests there was a resonance at very low frequencies (0.1 THz) in the 500 × 500 μm^2 sample. This resonance is at too low a frequency to be clearly resolved in our spectrometer but would be expected to show in measurements that can better resolve this frequency range. The charge-carrier densities varied from the experimentally calculated value ($5.4 \times 10^{17}\ cm^{-3}$) but were within expectations when accounting for differences in absorption and charge recombination between samples. Similar mobilities were calculated across all samples, despite significant differences in their photoconductivity spectra. It was known that the samples had similar properties, as they were fabricated from identically prepared films; hence, this result confirms that the surface plasmon model can separate the influence of sample geometry from the intrinsic carrier response in THz spectroscopy.

C. Plasmonic nature of the resonance

In Secs. II A and II B, we established an inverse relationship between the size of features in structured semiconductors and the frequency of geometric resonances. Here, we confirm that the resonances follow the plasmonic description of Nienhuys and Sundström,[25] and thus our observations can be generally applied to plasmonic resonances in other material systems. A series of photoconductivity measurements were conducted on the 7 × 7 μm^2 microsquares over a range of different photoexcitation intensities (0.3 to 23.6 $\mu J\ cm^{-2}$), and the spectra are shown in Fig. 5(a). There is a significant increase in resonant frequency with increasing excitation fluence. Figure 5(c) shows that this increase in resonant frequency is proportional to the square root of the charge-carrier density, a clear signature of plasmons [Eq. (2)].

We support our experimental measurements with FDTD simulations. Figure 5(b) shows the conductivity spectra from simulations of a single 7 × 7 μm^2 microsquare at charge-carrier densities ranging from 1×10^{16} to $9 \times 10^{17}\ cm^{-3}$ (line color changes from blue to red as carrier density increases, as indicated by the arrow). The simulations also show the increase in resonant frequency with the square root of the charge-carrier density [Fig. 5(c)] that was observed in the experiments, except with an offset of a factor of two. This

TABLE III. Material characteristics extracted by fitting the surface plasmon model to the THz photoconductivity spectra shown in Fig. 4.

Sample	N ($\times 10^{17}\ cm^{-3}$)	$\omega_0/2\pi$ (THz)	μ ($cm^2\ V^{-1}\ s^{-1}$)
Film	3.5 ± 0.3	0	3700 ± 500
500 × 500 μm^2	5.9 ± 0.1	0.1 ± 0.1	3000 ± 300
50 × 50 μm^2	6.6 ± 0.3	1.14 ± 0.01	3200 ± 100
7 × 7 μm^2	4.0 ± 0.1	3.7 ± 0.1	2800 ± 200

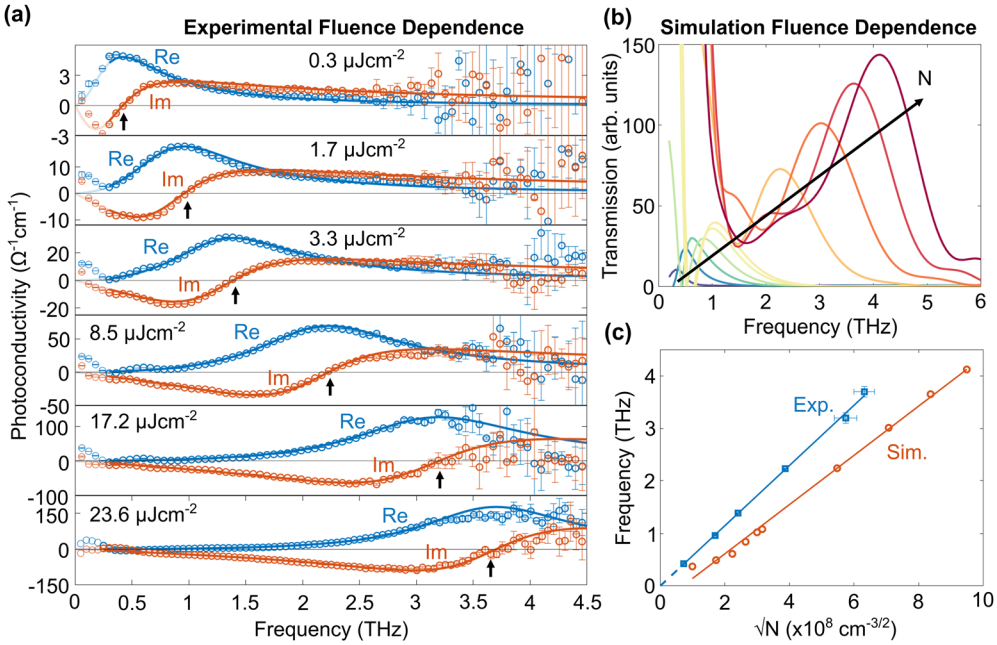

FIG. 5. (a) THz photoconductivity spectra of the 7 × 7 μm^2 microsquares measured ~8 ps after photoexcitation with 35-fs duration laser pulses with 800-nm center wavelength (E_{photon} = 1.55 eV) with fluences from 0.3 to 23.6 $\mu J\ cm^{-2}$. The circles are the measured data, and the solid lines are the fits to the surface plasmon model [Eq. (1)]. (b) Select photoconductivity spectra from FDTD simulations of a single 7 × 7 μm^2 microsquare at different charge-carrier densities. The arrow indicates the increasing resonant frequency with increasing charge-carrier density, N. (c) Plot of the resonant frequency against $\sqrt{N}$. The blue line shows the experimental relationship [data in (a)], while the red line shows the simulated relationship [data in (b)]. All measurements were performed at room temperature in a vacuum chamber at 0.1 mbar.

offset is likely because of differences in the background doping and optical absorption between the experiment and simulation. Yet, the good agreement between simulations and experiments strongly suggests a plasmonic origin to the microsquares resonance. Previous studies have identified the same trend in nanowires,[26,27] and so our findings in both nanowires and microsquares are examples of the same phenomena relating plasmonic resonant frequencies to their geometry.

III. CONCLUSIONS

In conclusion, we have investigated the influence of sample geometry on THz photoconductivity measurements. We observed the establishment of a plasmonic resonance that shifted to higher frequencies in GaAs nanowires and microsquares as the dimensions of the samples decreased. The photoconductivity spectra of the nanowires and microsquares were well-fitted by the surface plasmon model. For both systems, the charge-carrier mobility was successfully extracted, despite the significant differences in the THz photoconductivity spectra. Our results demonstrate the effectiveness of the surface plasmon model for analyzing spectra of structured semiconductors.

The relationship between structure size and geometric resonant frequency has important implications for the interpretation of THz measurements on structured materials. In particular, measurements of ensembles of elements with varying sizes, such as nanowires or grains, will cause a broadening of the geometric resonance that lowers the extracted mobility of the material. One must take care to recognize that the extracted mobility is a lower bound for the true mobility of the sample. Our FDTD simulations and fluence dependent measurements strongly indicate that the resonances in this study are plasmonic, and hence, the same size dependence is expected for other systems exhibiting such resonances. Overall, our results show the power of THz spectroscopy to accurately measure the electrical properties of structured materials, such as semiconducting particles, nanowires, and microscale grains in polycrystalline semiconductors.

SUPPLEMENTARY MATERIAL

The supplementary material details the experimental methods for fabricating the nanowires and microsquares, measuring the samples with THz spectroscopy, and developing the FDTD simulations. Then, enlarged SEM images of the nanowires along with their length histograms are provided. Finally, details on the THz data analysis, model fitting algorithm, and geometric factors are provided.

ACKNOWLEDGMENTS

We gratefully acknowledge support from the EPSRC (UK) under Grant Nos. EP/W018489/1 and EP/T025077/1. This work

was supported by the Australian Research Council (ARC) through the funding of the Center of Excellence for Transformative Meta-Optical Systems, Grant No. CE200100010. Access to the growth and fabrication facilities was made possible through the Australian National Fabrication Facility, ACT Node. J.C.B. thanks the Alexander von Humboldt Foundation for her Feodor Lynen Research Fellowship.

AUTHOR DECLARATIONS

Conflict of Interest

The authors have no conflicts to disclose.

Author Contributions

M.B.J., T.S., and K.P. designed the study and supervised the project. F.M.W., J.C.B., and T.J.K. conducted the measurements on the microgrid samples and all modeling and data analysis. T.H. fabricated the microsquare samples and performed all SEM measurements on the microsquares under the supervision of H.H.T. and C.J. D.A.D. performed THz spectroscopy measurements on the nanowire samples that were prepared by C.U. under the supervision of H.J., who also grew the nanowires. K.P. completed SEM and optical imaging of the nanowires. H.K. designed and built the custom data acquisition hardware and firmware used in all THz measurements. T.S. developed the numerical FDTD model. F.M.W. wrote the article with contributions from all authors.

Ford M. Wagner: Data curation (equal); Formal analysis (lead); Investigation (equal); Methodology (lead); Visualization (lead); Writing – original draft (lead); Writing – review & editing (equal). **Tuomas Haggren**: Data curation (equal); Formal analysis (supporting); Investigation (equal); Methodology (supporting); Writing – review & editing (equal). **Jasmin-Clara Bürger**: Data curation (equal); Formal analysis (supporting); Investigation (supporting); Methodology (supporting); Writing – review & editing (supporting). **Terng Junn Keat**: Data curation (supporting); Formal analysis (supporting); Investigation (supporting); Methodology (supporting); Writing – review & editing (supporting). **Kun Peng**: Data curation (supporting); Investigation (supporting); Methodology (supporting); Supervision (supporting). **Chawit Uswachoke**: Data curation (supporting); Investigation (supporting); Methodology (supporting); Writing – review & editing (supporting). **Djamshid A. Damry**: Data curation (supporting); Formal analysis (supporting); Investigation (supporting); Methodology (supporting). **Hans Kraus**: Data curation (supporting); Funding acquisition (supporting); Methodology (supporting); Software (lead); Writing – review & editing (supporting). **Hannah J Joyce**: Conceptualization (supporting); Data curation (supporting); Formal analysis (supporting); Investigation (supporting); Methodology (supporting); Supervision (equal); Writing – review & editing (supporting). **Hark Hoe Tan**: Data curation (supporting); Funding acquisition (equal); Investigation (supporting); Supervision (supporting); Writing – review & editing (supporting). **Chennupati Jagadish**: Funding acquisition (equal); Investigation (supporting); Supervision (supporting); Writing – review & editing (supporting). **Thomas Siday**: Conceptualization (equal); Data curation (equal); Formal analysis (equal); Investigation (equal); Methodology (equal); Supervision (equal); Writing – original draft (equal); Writing – review & editing (equal). **Michael B Johnston**: Conceptualization (equal); Funding acquisition (equal); Methodology (equal); Supervision (equal); Writing – review & editing (equal).

DATA AVAILABILITY

The data that support the findings of this study are available from the corresponding author upon reasonable request.

REFERENCES

[1] H. J. Joyce, J. L. Boland, C. L. Davies, S. A. Baig, and M. B. Johnston, Semicond. Sci. Technol. **31**, 103003 (2016).
[2] H. J. Joyce, C. J. Docherty, Q. Gao, H. H. Tan, C. Jagadish, J. Lloyd-Hughes, L. M. Herz, and M. B. Johnston, Nanotechnology **24**, 214006 (2013).
[3] J. L. Boland, G. Tütüncüoglu, J. Q. Gong, S. Conesa-Bog, C. L. Davies, L. M. Herz, A. F. I. Morral, and M. B. Johnston, Nanoscale **9**, 7839 (2017).
[4] J. L. Boland, A. Casadei, G. Tütüncüoglu, F. Matteini, C. L. Davies, F. Jabeen, H. J. Joyce, L. M. Herz, A. F. I. Morral, and M. B. Johnston, ACS Nano **10**, 4219–4227 (2016).
[5] C. S. Ponseca, Jr., H. Němec, J. Wallentin, N. Anttu, J. P. Beech, A. Iqbal, M. Borgström, M.-E. Pistol, L. Samuelson, and A. Yartsev, Phys. Rev. B **90**, 085405 (2014).
[6] A. M. Shaltout, V. M. Shalaev, and M. L. Brongersma, Science **364**, eaat3100 (2019).
[7] W. J. Padilla, A. J. Taylor, C. Highstrete, M. Lee, and R. D. Averitt, Phys. Rev. Lett. **96**, 107401 (2006).
[8] J. Gu, R. Singh, X. Liu, X. Zhang, Y. Ma, S. Zhang, S. A. Maier, Z. Tian, A. K. Azad, H.-T. Chen, A. J. Taylor, J. Han, and W. Zhang, Nat. Commun. **3**, 1151 (2012).
[9] M. R. Shcherbakov, S. Liu, V. V. Zubyuk, A. Vaskin, P. P. Vabishchevich, G. Keeler, T. Pertsch, T. V. Dolgova, I. Staude, I. Brener, and A. A. Fedyanin, Nat. Commun. **8**, 17 (2017).
[10] A. Fakharuddin, M. K. Gangishetty, M. Abdi-Jalebi, S.-H. A. R. D. N. Chinbin Mohd YusoffCongreve, W. Tress, F. Deschler, M. Vasilopoulou, H. J. Bolink, M. Vasilopoulou, and H. J. Bolink, Nat. Electron. **5**, 203–216 (2022).
[11] M. B. Johnston and L. M. Herz, Acc. Chem. Res. **49**, 146–154 (2016).
[12] H. D. Kim, H. Ohkita, H. Benten, and S. Ito, Adv. Mater. **28**, 917–922 (2016).
[13] K. Storm, F. Halvardsson, M. Heurlin, D. Lindgren, A. Gustafsson, P. M. Wu, B. Monemar, and L. Samuelson, Nat. Nanotechnol. **7**, 718–722 (2012).
[14] P. U. Jepsen, D. G. Cooke, and M. Koch, Laser Photonics Rev. **5**, 124–166 (2011).
[15] R. Ulbricht, E. Hendry, J. Shan, T. F. Heinz, and M. Bonn, Rev. Mod. Phys. **83**, 543 (2011).
[16] C. A. Schmuttenmaer, Chem. Rev. **104**, 1759–1779 (2004).
[17] G. M. Turner, M. C. Beard, and C. A. Schmuttenmaer, J. Phys. Chem. B **106**, 11716–11719 (2002).
[18] M. C. Beard, G. M. Turner, J. E. Murphy, O. I. Micic, M. C. Hanna, A. J. Nozik, and C. A. Schmuttenmaer, Nano Lett. **3**, 1695–1699 (2003).
[19] J. L. Boland, F. Amaduzzi, S. Sterzl, H. Potts, L. M. Herz, A. Fontcuberta i Morral, and M. B. Johnston, Nano Lett. **18**, 3703–3710 (2018).
[20] V. Pushkarev, H. Němec, V. C. Paingad, J. Maňák, V. Jurka, V. Novák, T. Ostatnický, and P. Kužel, Adv. Funct. Mater. **32**, 2107403 (2022).
[21] M. V. Exter and D. Grischkowsky, Appl. Phys. Lett. **56**, 1694–1696 (1990).
[22] D. Grischkowsky, S. Keiding, M. V. Exter, and C. Fattinger, J. Opt. Soc. Am. B **7**, 2006–2015 (1990).
[23] P. Kužel and H. Němec, Adv. Opt. Mater. **8**, 1900623 (2020).
[24] P. Kužel and H. Němec, J. Phys. D: Appl. Phys. **47**, 374005 (2014).
[25] H.-K. Nienhuys and V. Sundström, Appl. Phys. Lett. **87**, 012101 (2005).
[26] P. Parkinson, J. Lloyd-Hughes, Q. Gao, H. H. Tan, C. Jagadish, M. B. Johnston, and L. M. Herz, Nano Lett. **7**, 2162–2165 (2007).
[27] P. Parkinson, H. J. Joyce, Q. Gao, H. H. Tan, X. Zhang, J. Zou, C. Jagadish, L. M. Herz, and M. B. Johnston, Nano Lett. **9**, 3349–3353 (2009).

[28]M. B. Johnston and H. J. Joyce, Prog. Quantum Electron. **85**, 100417 (2022).
[29]S. A. Baig, J. L. Boland, D. A. Damry, H. H. Tan, C. Jagadish, H. J. Joyce, and M. B. Johnston, Nano Lett. **17**, 2603–2610 (2017).
[30]L. Balaghi, S. Shan, I. Fotev, F. Moebus, R. Rana, T. Venanzi, R. Hübner, T. Mikolajick, H. Schneider, M. Helm, A. Pashkin, and E. Dimakis, Nat. Commun. **12**, 6642 (2021).
[31]H. J. Joyce, S. A. Baig, P. Parkinson, C. L. Davies, J. L. Boland, H. H. Tan, C. Jagadish, L. M. Herz, and M. B. Johnston, J. Phys. D: Appl. Phys. **50**, 224001 (2017).
[32]L. W. Chou, N. Shin, S. V. Sivaram, and M. A. Filler, J. Am. Chem. Soc. **134**, 16155–16158 (2012).
[33]J. Schindelin, I. Arganda-Carreras, E. Frise, V. Kaynig, M. Longair, T. Pietzsch, S. Preibisch, C. Rueden, S. Saalfeld, B. Schmid, J.-Y. Tinevez, D. J. White, V. Hartenstein, K. Eliceiri, P. Tomancak, and A. Cardona, Nat. Methods **9**, 676–682 (2012).
[34]W. L. Barnes, Am. J. Phys. **84**, 593–601 (2016).
[35]O. Madelung, *Semiconductors—Basic Data* (Springer, Berlin, Heidelberg, 1996).
[36]M. C. Beard, G. M. Turner, and C. A. Schmuttenmaer, Phys. Rev. B **62**, 15764 (2000).